A Practical Approach to Model a Cable with Nonlinear Material Characteristics

Ganjavi, Amir; Zare, Firuz; Kumar, Dinesh; Abbosh, Amin; Konstanty, Bialkowski; Davari, Pooya

Published in:
2021 IEEE 19th International Power Electronics and Motion Control Conference (PEMC)

DOI (link to publication from Publisher):
10.1109/PEMC48073.2021.9432586

Publication date:
2021

Document Version
Accepted author manuscript, peer reviewed version

A Practical Approach to Model a Cable with Nonlinear Material Characteristics

Amir Ganjavi
School of ITEE
The University of Queensland
Brisbane, Australia
Email: a.ganjavi@uq.net.au

Firuz Zare
School of ITEE
The University of Queensland
Brisbane, Australia
Email: f.zare@uq.edu.au

Dinesh Kumar
Global Research and Development Center
Danfoss Drives A/S
Gråsten, Denmark
Email: dineshr30@ieee.org

Amin Abbosh
School of ITEE
The University of Queensland
Brisbane, Australia
Emial: a.abbosh@uq.edu.au

Bialkowski Konstanty
School of ITEE
The University of Queensland
Brisbane, Australia
Email: ksb@itee.uq.edu.au

Pooya Davari
Department of Energy Technology
Aalborg University
Aalborg, Denmark
Email: pda@et.aau.dk

***Abstract*—This paper proposes a practical method to model the Common-Mode (CM) impedance of power cable in Finite Element Analysis (FEA) software. The proposed approach utilizes a reverse-engineering method to estimate the frequency-dependent characteristics of the cable materials. Accordingly, two experimental measurements are proposed to calculate the parameters of the cable assumed from a basic lumped-π model. Then the material specifications of the cable PVC are estimated in the FEA software. The results verify that the the proposed model can predict the CM impedance of the cable with a great accuracy in a wide frequency range. This approach is highly practical and convenient, which can be readily extended to different kinds of power cables, ensuring high accuracy at a wide frequency range.**

I. Introduction

Nowadays, electric-motor driven systems consume more than 40% of the worldwide energy [1]. As a result, Adjustable Speed Drives (ASDs) play an important role in energy generation for today's industrial world [2]–[4]. As shown in Fig. 1, in the typical applications of a three-phase ASD, power cable is used as a feeding interface between the motor and drive. According to Fig. 1, $i_{PE-Motor}$ and $i_{PE-Cable}$ are the Common-Mode (CM) currents flowing to the ground due to the motor and cable parasitic couplings, respectively; therefore, i_{Eq} comprises the equivalent CM current due to $i_{PE-Motor}$ and $i_{PE-Cable}$. Recently, due to the growing tendency to increase the switching frequency of the power converters, parasitic couplings of the cables can significantly affect the Electromagnetic Compatibility (EMC) performance in the drive systems [5]–[7]. In fact, power cables can significantly reduce the CM impedance seen from the motor side, making the system more susceptible to Electromagnetic Interference (EMI) emissions [8].

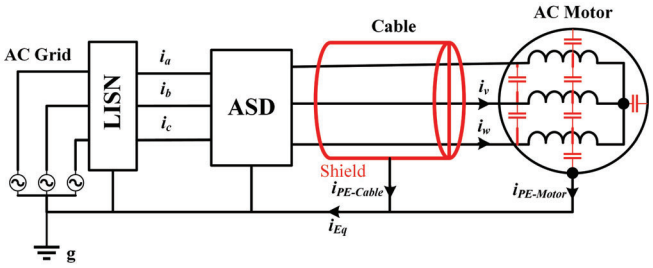

Fig. 1. A typical ASD including its power cable.

Due to the frequency-dependent characteristics of permeability, permittivity and skin depth, simple cable models are not able to achieve high accuracy [9]. As an example, due to the frequency-dependency of skin effect, the conduction losses increase with frequency, resulting in discrepancies between the measured impedance and the simple linear models [10]. So far, numerous cable models have been proposed in the literature [9], [11]–[14]. In [9], Wang, *et al.* proposed a cable model useful for over-voltage prediction. In order to improve the accuracy of the model, the authors utilized a high-order multiple-π sections. However, this will complicate the model, leading to the complex equations to extract the parameters. Consequently, transmission-line modeling (TLM) approach has been utilized to solve the equations. In [12], a transmission line model of a power cable has been achieved through Maxwell 2D Finite Element Analysis (FEA). The literature suggests a practical method to model a power cable through FEA software. Although the model suggests a good accuracy for predicting the cable impedance, deviations can be seen between the models and measurements. These deviations

could be attributed to the limited accuracy of FEA simulations. Moreover, modeling the complex geometrical structures of cables and the the materials used for them is usually hard to implement in the finite-element software.

In this paper, a highly practical method is proposed to extract the CM model of a power cable. The proposed method is a reverse-engineering approach, based on synthesise of the approximating calculations and experimental measurements. Accordingly, at the first step, two test measurements are suggested to extract the inductive and capacitive CM impedances of the cable. Secondly, the parameters of the cable are calculated based on a simple basic lumped-π model. In the next step, the frequency-dependent material characteristics of the cable PVCs are estimated based on the approximating calculations in ANSYS 2D Extractor. The simulation results validate that through the proposed method, the CM impedance of the cable can be predicted with a great accuracy at a wide frequency range. Also, the suggested approach can be readily extended to different kinds of power cables.

II. Measurements and Calculations

Fig. 2 shows the general cross-section of a shielded cable analyzed in this paper. According to Fig. 2, the cable under study includes three active wires as R, S and T; and a ground wire as the protective earth (PE). Moreover, Fig. 2 depicts the capacitive couplings of the cable, which can be defined with: C_{ws} as the capacitive couplings between the wires and shield, C_{ww1} as the capacitive couplings between the adjacent wires, and C_{ww2} as the capacitive couplings between the diagonal wires.

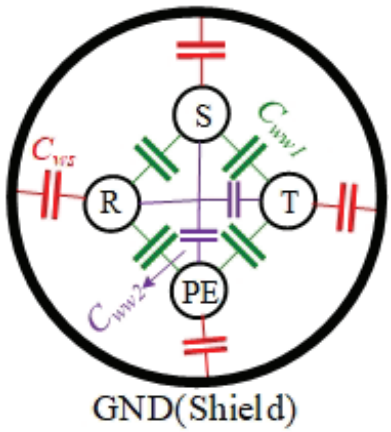

Fig. 2. Cross-section of a cable including its capacitive couplings.

In order to conveniently approximate the parameters of the power cable, a basic lumped-π model has been used as the criterion (see Fig. 4). Subsequently, to extract the CM lumped parameters of the cable model, two test measurements have been conducted, named as Tests A and B. According to Fig. 3, Tests A and B are conducted to extract the inductive and capacitive characteristics of the cable, respectively. As shown in Fig. 3, in Test A, the far end wires of R', S', T', PE' and shield are all connected together, while in Test B, the shield is not connected with the far end wires. Consequently, Figs. 4 (a) and (b) depict the low-frequency equivalent CM circuits of the benchmark lumped-π model for Tests A and B, respectively. According to Fig. 4, the lumped parameters of R_s, L_s, C_{ws}, and R_{ws} represent the equivalent series resistance, series inductance, shunt capacitor, and leakage resistance of power cable, respectively.

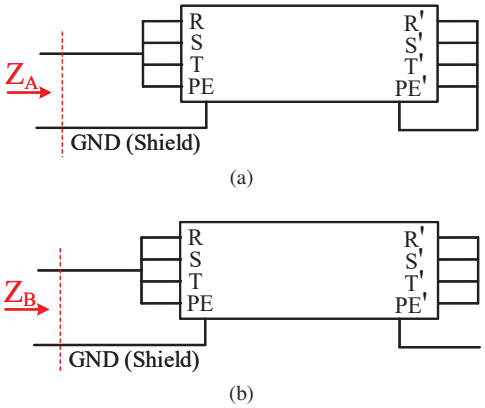

Fig. 3. Measurement configurations. (a) Test A, (b), Test B.

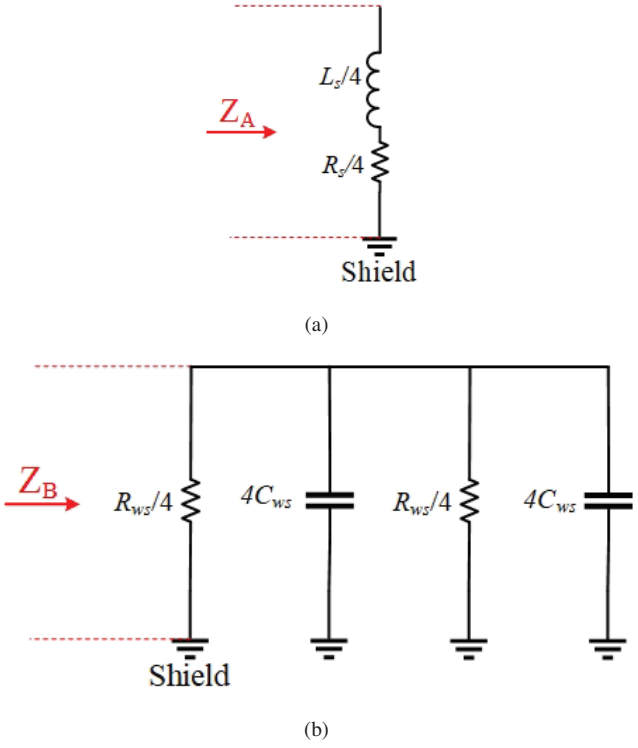

Fig. 4. Equivalent CM circuits of the basic lumped-π model at low-frequency. (a) Test A, (b), Test B.

A. Extracting R_s and L_s Through Test A

According to Figs. 3 (a) and 4 (a), the parameters R_s and L_s can be calculated through Test A. Consequently, these parameters can be estimated based on the low-frequency equivalent

TABLE I
CALCULATED CM PARAMETERS FOR THE LUMPED π CABLE MODEL AT 100 HZ

Parameter	L_s	R_s	C_{ws}	R_{ws}
Value	57.29 μH	2.78 Ω	7.53 nF	3.78 MΩ

circuit of the lumped model (see Fig. 4 (a)). Accordingly, R_s and L_s can be calculated at low-frequencies through (1):

$$Z_A = \frac{R_s}{4} + \frac{sL_s}{4} \tag{1}$$

where Z_A is the cable impedance measured through Test A (see Figs. 3 (a)), and s=$j\omega$, where ω is the angular frequency.

B. Extracting R_{ws} and C_{ws} Through Test B

According to Figs. 3 (b) and 4 (b), the parameters R_{ws} and C_{ws} can be calculated through Test B. Consequently, these parameters can be estimated based on the low-frequency equivalent circuit of the lumped model (see Fig. 4 (b)). Accordingly, R_{ws} and C_{ws} can be calculated at low-frequencies through (2):

$$Z_B = \frac{sR_{ws}}{8C_{ws}(\frac{R_{ws}}{8} + \frac{s}{C_{ws}})} \tag{2}$$

According to (1) and (2), Table I depicts the calculated parameters of the lumped-π cable model at 100 Hz. With the same procedure, the parameters of the model can be calculated at different frequency points. Accordingly, Figs. 5 and 6 show the comparison between the lumped-π model calculated at 100 Hz and the measured experimental impedance through Tests A and B, respectively. As can be seen in Figs. 5 and 6, the calculated impedances deviate from the experimental measurements at higher frequencies. This could be attributed to the fact that the model is calculated at 100 Hz and due to the frequency-dependency of the cable couplings in the real-life case, deviations occur at higher frequencies. In fact, the simple lumped-π model calculated at a single frequency point is not able to predict the CM impedance behavior of the cable at a wide frequency range. Therefore, in order to solve this issue, it is explained how a cable can be modeled in ANSYS software, considering the frequency-dependent characteristics of the material.

III. MODELING IN ANSYS SOFTWARE

As discussed above, due to the frequency dependency of relative permeability and permittivity, the simple lumped model is not able to predict the CM impedance of the cable at a wide frequency range. Consequently, in this section, it is explained how a cable can be modeled in ANSYS software to improve the accuracy at a wide range of frequency.

A. Extracting the Frequency-Dependent Characteristics

Fig. 7 (a) shows the cable analyzed for this paper. The length of the cable is 100 m, and it includes PVC insulation, PVC inner and outer sheaths, and a shield made up of tinned-copper

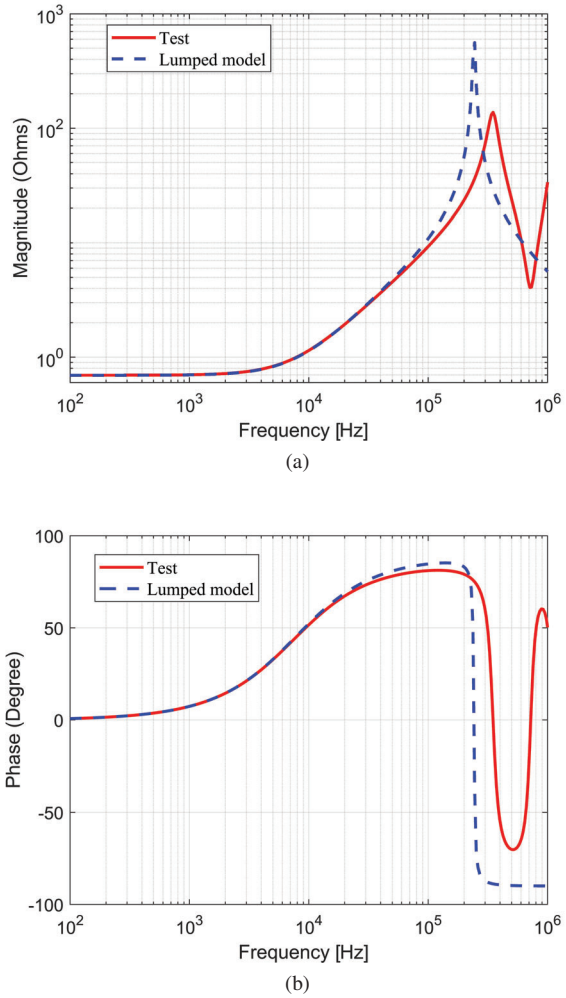

Fig. 5. Measured and calculated CM impedance of the lumped π model at 100 Hz through Test A (cable length is 100 m). (a) Magnitude, (b) phase.

braiding. Moreover, the cores of the cable are twisted in layers, which is not included in the model. Subsequently, Fig. 7 (b) shows this cable modeled in ANSYS 2D Extractor software.

In order to assign the frequency-dependent permeability and permittivity for the PVC in ANSYS 2D Extractor, a reverse-engineering technique has been utilized based on the calculated and measured impedances of the cable. In fact, according to (1) and (2), the parameters of the cable are calculated at several frequency points. According to Figs. 5 and 6, these calculations can be conducted up to around 110 kHz, where the the phases of impedances for Tests A and B are almost +90 and -90 degrees, respectively. This could be attributed to the fact that up to this frequency range, the low-frequency approximations of (1) and (2) are reasonably accurate, while at higher frequencies, the accuracy of approximations will degrade.

In order to match the measured impedances with ANSYS simulation results, the experimental frequency-dependent permittivity of the cable's PVC should be assigned in the simulations. The frequency-dependent permittivity of the cable

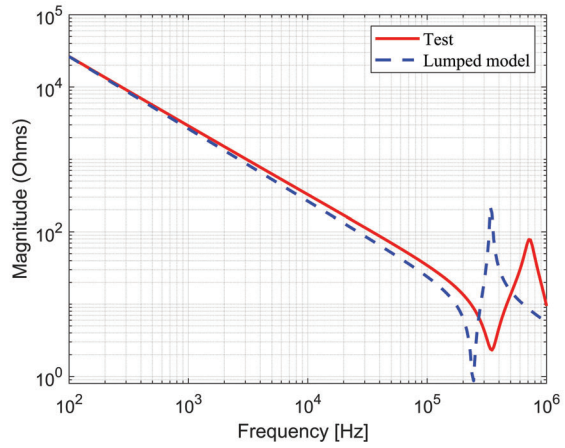

(a)

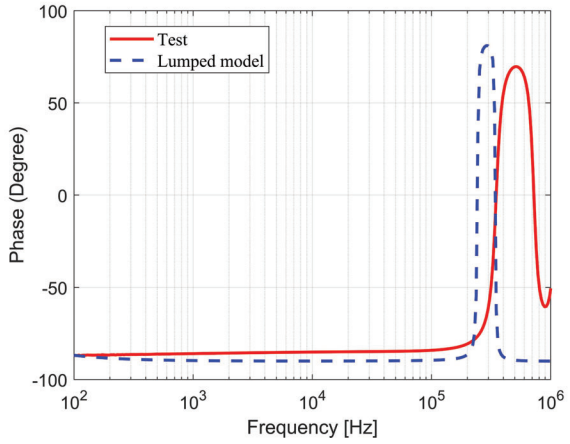

(b)

Fig. 6. Measured and calculated CM impedance of the lumped π model at 100 Hz through Test B (cable length is 100 m). (a) Magnitude, (b) phase.

can be estimated based on calculations of C_{ws} at different frequencies through (1) and (2) (see Table I for the calculated values at 100 Hz as an example). Moreover, it is clear that C_{ws} can be also calculated according to (3), assuming the capacitance for flat-plates:

$$C_{ws} = \varepsilon_0 \varepsilon_r \frac{A}{d} \tag{3}$$

where ε_0 is the vacuum permittivity, ε_r is the relative permittivity of dielectric insulator, A is the common area between the conductors, and d is the distance between the conductors. According to (3), the permittivity of PVC material has a direct relation with C_{ws}. Hence, by drawing a comparison between the calculated values of C_{ws} through (1) and (2) at different frequency points and the ones initially calculated by ANSYS solver, the permittivity of PVC material should be refined based on appropriate coefficients. In fact, these refining coefficients can be readily extracted by comparing the the calculated values of C_{ws} through (2), the calculated values of C_{ws} through the ANSYS solver, and the equation (3). With the same scenario, the frequency-dependent permeability will be extracted based on calculations of L_s through (1). Consequently, Fig. 8 depicts the estimated frequency-dependent permeability and permittivity of the PVC material with the proposed technique.

Moreover, Figs. 9 and 10 show the comparisons between the experimental test measurements and the model achieved in ANSYS software for Tests A and B, respectively. As can be seen in Figs. 9 and 10, the model achieved in the software is highly accurate at a wide frequency range, even at two different test configurations.

(a)

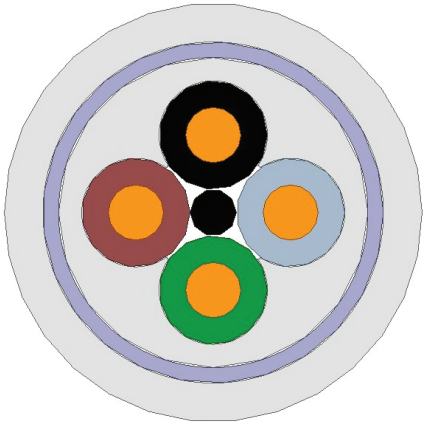

(b)

Fig. 7. (a) Cable under study [15], (b) Model in ANSYS 2D Extractor.

B. Time-Domain Analysis

After assigning the frequency-dependant characteristics of the cable PVCs in ANSYS 2D Extractor, the cable parameters are calculated by the software's solver at each sweeping frequency. Subsequently, the Scattering-matrix (S-matrix) of the cable will be derived through the software. In the next step, in order to analyze the cable in time-domain simulations, the equivalent circuit of the cable will be linked to ANSYS Simplorer based on the calculated Scattering-parameters (S-parameters) in ANSYS 2D Extractor. It is worth mentioning that the accuracy of the equivalent model in ANSYS Simplorer software depends on the number of orders and the error tolerance assigned to enforce passivity in the simulation.

Fig. 11 describes the simulation platform utilized in ANSYS Simplorer. According to Fig. 11, the multi-physics platform includes correlations between different sub-systems in ANSYS Software. Accordingly, a DC-choke with a frequency-dependent core material solved in ANSYS Maxwell [8], a parasitic model of AC machine [16], and the proposed cable

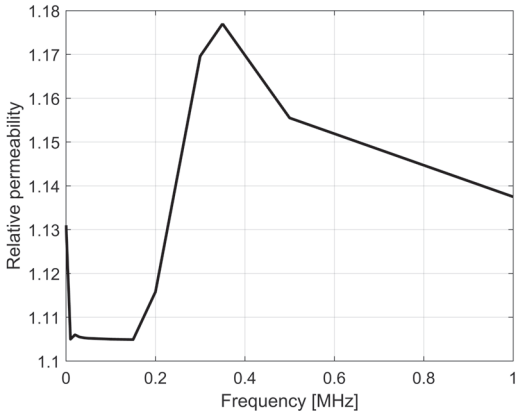

(a)

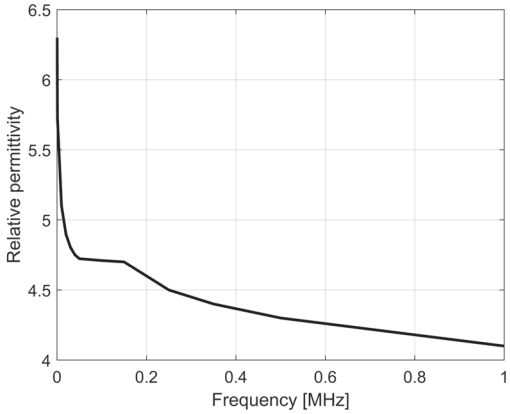

(b)

Fig. 8. Estimated frequency-dependent material characteristic assigned for cable PVC in ANSYS 2D Extractor. (a) Relative permeability, (b) relative permittivity.

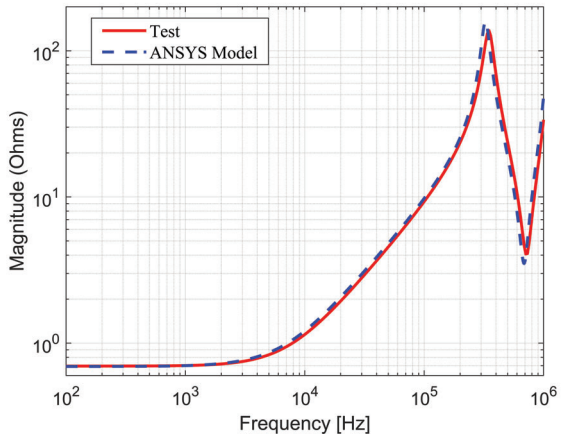

(a)

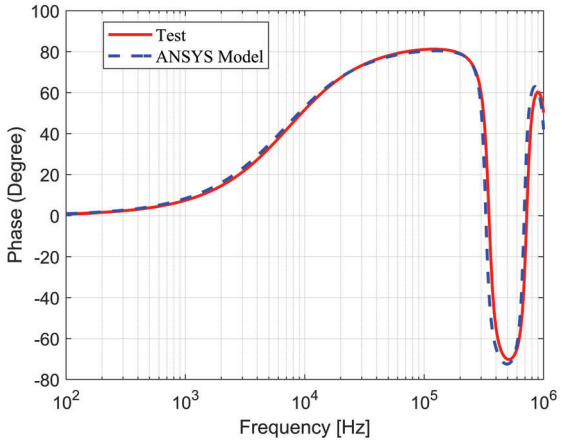

(b)

Fig. 9. Comparison between the experimental test measurements and the model achieved in ANSYS software for Test A (a) Magnitude, (b) Phase.

solved in ANSYS 2D Extractor are all linked to ANSYS Simplorer for the time-domain analysis. Moreover, the parameters of the drive are depicted in Table II. According to Table II, the switching frequency (f_{sw}) of the inverter is 5 kHz, and the drive is investigated under the rated power of 5 kW.

TABLE II
PARAMETERS OF ASD (SEE FIG. 11)

Parameters	L_{dc}, C_{dc}	L_{cm}	f_{sw}	Rated Power
Values	1.25 mH, 1 mF	5.3 mH	5 kHz	5 kW

In order to highlight the effect of cable, Fig. 12 compares the simulation results between when cable model is assigned in the system and when the cable is removed. Accordingly, Fig. 12 (a) shows the grid current i_a and Fig. 12 (b) depicts i_{Eq} (see Fig. 1), with and without the cable assigned in the system. As can be seen in Fig. 12, cable can have a considerable effect on the impedance of the drive, addressing its importance for CM noise analysis of the system. According to Fig. 12 (a), when cable is assigned in the system, the grid current is reduced. On the other hand, according to Fig. 12 (b), when cable is assigned in the system, i_{Eq} increases, injecting extra CM current to the system. This could be attributed to the fact that cable decreases the CM impedance of the system.

In Fig. 13, the effect of cable on the current harmonics at the grid side is investigated at different inductance values of DC chokes. Accordingly, in order to have a better power quality analysis, the FFT spectrum of the grid current i_a has been normalized by dividing the currents to their fundamental current for each condition. Accordingly, it can be clearly seen in Fig. 13 that cable caused an increase in the harmonic emissions at the grid side. Consequently, when the inductance value of L_{dc}=1.25 mH is assigned for the DC chokes, the Total Harmonic Distortion (THD) of i_a is 54% and 45.3% with and without cable in the system, respectively. Moreover, when the inductance value of L_{dc}=2.25 mH is assigned for the DC chokes, the THD of i_a is 39.5% and 35.8% with and without cable in the system, respectively.

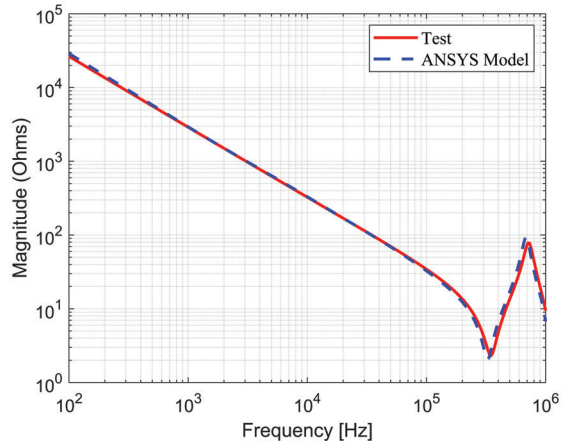

(a)

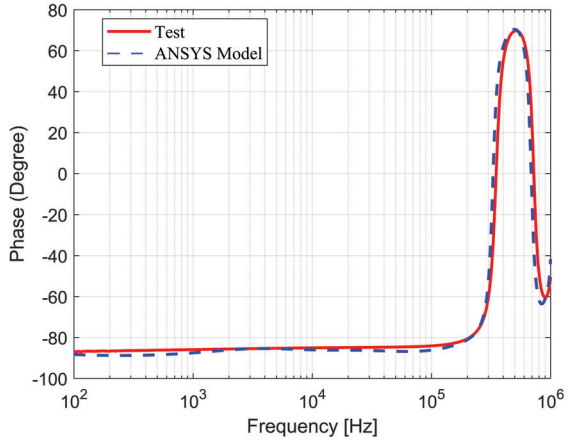

(b)

Fig. 10. Comparison between the experimental test measurements and the model achieved in ANSYS software for Test B (a) Magnitude, (b) Phase.

IV. Conclusion

This paper proposed a systematic approach to model a power cable in FEA software. The proposed approach is a reverse-engineering method, based on approximating calculations and test measurements. Firstly, two test measurements have been proposed to calculate the basic lumped-π parameters of the cable through approximating calculations. Then the relative permeability and permittivity of PVC materials are predicted with the help of ANSYS software and the approximating calculations. After assigning the frequency-dependent features of cable materials in ANSYS 2D Extractor, the software solves the S-parameters of the cable model in the frequency-domain. Finally, the model can be utilized in the time-domain simulations through the state-space dynamic couplings of the S-parameters. The results verify that the proposed method is highly useful for accurately predicting the impedance of power cables at a wide frequency range.

Acknowledgment

The authors would like to thank the Australian Research Council, supporting FT150100042 and LP170100902 projects.

References

[1] P. Waide and C. U. Brunner, "Energy efficiency policy opportunities for electric motor-driven systems," *International Energy Agency (IEA)*, 2011.

[2] H. Rathnayake, A. Ganjavi, F. Zare, D. Kumar, and P. Davari, "Common-mode noise modelling and resonant estimation in a three-phase motor drive system: 9-150 khz frequency range," in *2020 22nd European Conference on Power Electronics and Applications (EPE'20 ECCE Europe)*, 2020, pp. 1–10.

[3] Y. Li, H. Lin, H. Huang, C. Chen, and H. Yang, "Analysis and performance evaluation of an efficient power-fed permanent magnet adjustable speed drive," *IEEE Transactions on Industrial Electronics*, vol. 66, no. 1, pp. 784–794, Jan 2019.

[4] U. Choi, S. Jørgensen, and F. Blaabjerg, "Impact of cooling system capacity on lifetime of power module in adjustable speed drives," *IEEE Journal of Emerging and Selected Topics in Power Electronics*, vol. 7, no. 3, pp. 1768–1776, Sep. 2019.

[5] *Broadband Behavior of Fundamental Components of ASD*. John Wiley & Sons, Ltd, 2018, ch. 6, pp. 137–202. [Online]. Available: https://onlinelibrary.wiley.com/doi/abs/10.1002/9781119388975.ch6

[6] M. Moreau, N. Idir, and P. Le Moigne, "Modeling of conducted emi in adjustable speed drives," *IEEE Transactions on Electromagnetic Compatibility*, vol. 51, no. 3, pp. 665–672, 2009.

[7] E. J. Bartolucci and B. H. Finke, "Cable design for pwm variable-speed ac drives," *IEEE Transactions on Industry Applications*, vol. 37, no. 2, pp. 415–422, 2001.

[8] A. Ganjavi, H. Rathnayake, F. Zare, D. Kumar, A. Abbosh, and P. Davari, "Investigating the effect of different parameters on harmonics and emi emissions at the frequency range of 0–9 khz," in *2020 22nd European Conference on Power Electronics and Applications (EPE'20 ECCE Europe)*, 2020, pp. P.1–P.10.

[9] L. Wang, C. Ngai-Man Ho, F. Canales, and J. Jatskevich, "High-frequency modeling of the long-cable-fed induction motor drive system using tlm approach for predicting overvoltage transients," *IEEE Transactions on Power Electronics*, vol. 25, no. 10, pp. 2653–2664, 2010.

[10] *Broadband Behavior of Fundamental Components of ASD*. John Wiley & Sons, Ltd, 2018, ch. 6, pp. 137–202. [Online]. Available: https://onlinelibrary.wiley.com/doi/abs/10.1002/9781119388975.ch6

[11] Y. Weens, N. Idir, R. Bausiere, and J. J. Franchaud, "Modeling and simulation of unshielded and shielded energy cables in frequency and time domains," *IEEE Transactions on Magnetics*, vol. 42, no. 7, pp. 1876–1882, 2006.

[12] G. Skibinski, R. Tallam, R. Reese, B. Buchholz, and R. Lukaszewski, "Common mode and differential mode analysis of three phase cables for pwm ac drives," in *Conference Record of the 2006 IEEE Industry Applications Conference Forty-First IAS Annual Meeting*, vol. 2, 2006, pp. 880–888.

[13] A. F. Moreira, T. A. Lipo, G. Venkataramanan, and S. Bernet, "High-frequency modeling for cable and induction motor overvoltage studies in long cable drives," *IEEE Transactions on Industry Applications*, vol. 38, no. 5, pp. 1297–1306, 2002.

[14] H. Chen, Y. Yan, and H. Zhao, "Extraction of common-mode impedance of an inverter-fed induction motor," *IEEE Transactions on Electromagnetic Compatibility*, vol. 58, no. 2, pp. 599–606, 2016.

[15] *Power and control cables*, LAPP. [Online]. Available: https://www.lappkabel.com/cpr.html

[16] A. Ganjavi, H. Rathnayake, F. Zare, D. Kumar, J. Yaghoobi, P. Davari, and A. Abbosh, "Common-mode current prediction and analysis in motor drive systems for the new frequency range of 2–150 khz," *IEEE Journal of Emerging and Selected Topics in Power Electronics*, pp. 1–1, 2020.

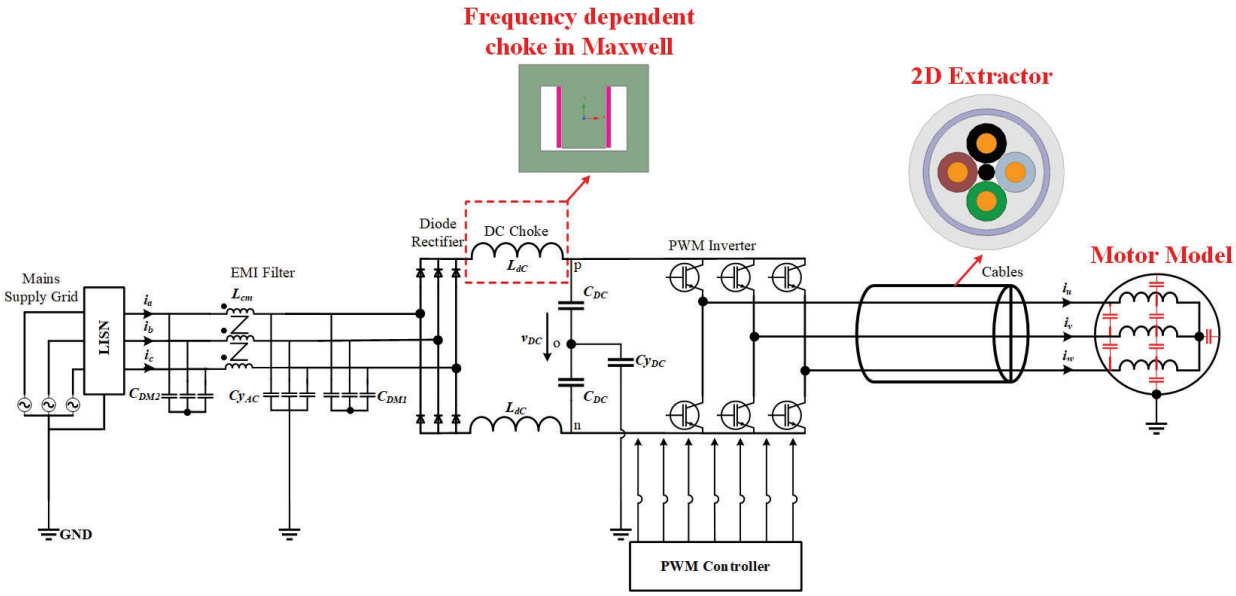

Fig. 11. Simulation platform in ANSYS Simplorer, including the frequency dependent DC-choke and cable.

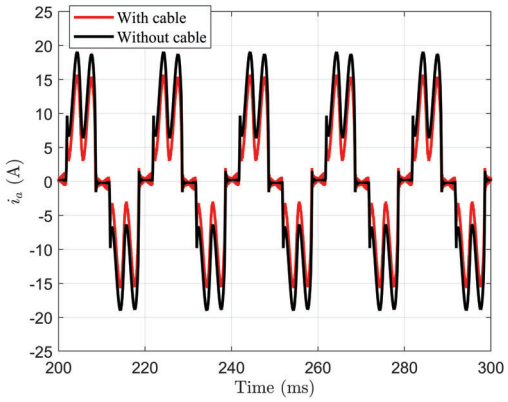

(a)

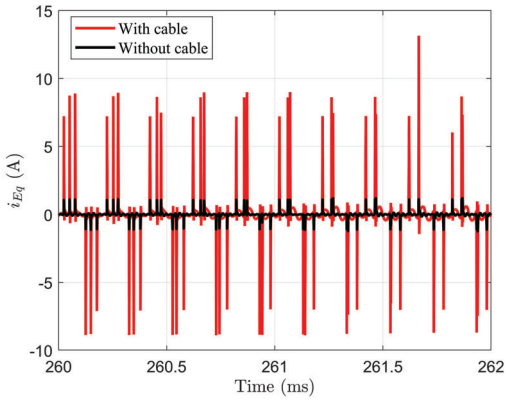

(b)

Fig. 12. Comparison of Simplorer simulation results between when the cable is assigned in the system and when it is removed (with output power of around 5 kW). (a) Grid current (i_a), (b) equivalent CM current (i_{Eq}).

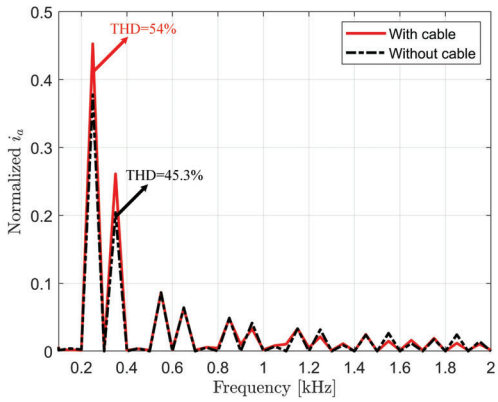

(a)

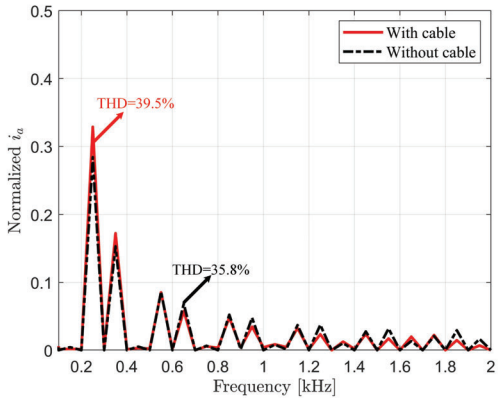

(b)

Fig. 13. Effect of cable at different inductance values of DC chokes. (a) L_{dc}=1.25 mH, (b) L_{dc}=2.25 mH.